

Photographic High-Dynamic-Range Scalar Visualization: Supplemental Material

Category: Research

ABSTRACT

This supplemental material contains contents that are left out from the paper for conciseness. Specifically, details of the tone-mapping operator evaluations (Section 3.1 of the paper) are explained, including the full set of tone-mapped images used in evaluations of tone-mapping operators, and details of selected distortion images.

1 EVALUATIONS OF TONE MAPPING OPERATORS

This section reports on the details of the evaluation of tone-mapping operators which is discussed in Section 3.1 of the paper. The evaluation was performed using three representative HDR datasets: Hurricane Isabel 2D scatter plot (Isabel TvP), world flight routes (World Flights), and parallel coordinates of hurricane Isabel (Isabel parallel coordinates). These datasets are chosen because they are typical representatives of HDR data containing different types of features: Isabel TvP contains only dots; Isabel parallel coordinates contain curves and high-value area of curve crossings; the world flights data is a less abstract geospatial data containing both dots and curves.

Our systematic evaluation considers 14 popular tone-mapping operators: linear, gamma 1/2.2 (gamma), logarithmic (log), Ash02 [1], Pat00 [11], Man06 [10], Man08 [8], Mai11 [7], Fer11 [6], Fat02 [5], Dra03 [3], Dur02 [4], Rei02 [13], and Rei05 [12]. The tone-mapping operators are chosen to be evaluated as they are well-accepted techniques and have been implemented in the state-of-the-art HDR processing toolkit [9].

All tone-mapped LDR images used in the tone-mapping operator evaluation are shown in Figure 1. Names of tone-mapping techniques are shown in the first column; results of the World Flight data, Hurricane Isabel Parallel Coordinates, and Isabel TvP are listed in the second through fourth columns respectively.

The mean values of distortions of evaluated tone-mapping operators on each dataset and the average across all datasets are summarized in Table 1 in ascending order.

Table 1: Mean distortion metric of tone-mapping operators in our evaluation.

TMO	IsabelTvP	World Flights	IsabelPC	Averaged
Man08 [8]	0.483	0.372	0.698	0.517
Man06 [10]	0.541	0.796	0.558	0.632
Mai11 [7]	0.532	0.610	1.076	0.739
Ash02 [1]	0.749	1.653	0.731	1.044
Rei05 [12]	0.650	0.685	1.850	1.062
log	0.756	0.954	1.604	1.105
Dur02 [4]	0.803	1.211	1.632	1.216
Fat02 [5]	0.802	1.350	1.645	1.266
Fer11 [6]	1.267	1.666	1.681	1.538
Dra03 [3]	1.280	1.838	1.590	1.570
Pat00 [11]	1.339	1.684	1.696	1.573
Rei02 [13]	1.259	1.792	1.781	1.610
gamma	1.564	1.801	1.962	1.775
linear	2.580	2.663	2.626	2.623

The top three best performers (Man08 [8], Man06 [10], and Mai11 [7]) have much lower scores than other tone-mapping operators, indicating that they generate fewer distortions in general. Since

Mai11 [7] is the only global tone-mapping operator within the top three, we pick it as our choice for global HDR visualization. A further examination on the distributions of distortions in tone-mapped images made us choose Man06 [10] over Man08 [8] as Man06 [10] yields lower errors in regions of important features than Man08 [8].

Detailed distortion images of individual channels comparing the top three tone-mapping operators: [8], [10], and [7] are shown in Figure 2. The top three best performers (Man08 [8], Man06 [10], and Mai11 [7]) have much lower scores than other tone-mapping operators indicating that they generate fewer distortions in general. Therefore, we focus on these three tone-mapping operators and further examine the distribution of distortions in tone-mapped images generated by them. Figure 2 shows the case of the World Flight data where the distortion of Man08 [8] is significantly lower than the other two tone-mapping operators. The distortion maps are generated using [2], where green indicates loss of visible contrast, red for reversal of visible contrast, and blue for amplification of invisible contrast. By examining the distortion maps, it can be seen that the loss of contrast in Man08 [8] and Mai11 [7] occur particularly in high-value regions of the map, i.e., East Asia, Europe, and North America, making it difficult to recognize details in these regions; whereas the same type of distortion in Man06 [10] occurs in regions of lower values and of smaller distortion values. Although Man06 [10] yields higher error values in larger areas than the other tone-mapping operators for contrast reversal and amplification, these errors occur on regions of lower-value, and the features in those regions can still be seen in the tone-mapped image. These findings can be verified by examining the actual tone-mapped images (Figure 1).

REFERENCES

- [1] M. Ashikhmin. A tone mapping algorithm for high contrast images. In *Proceedings of the 2002 Eurographics Workshop on Rendering*, pp. 145–156, 2002. doi: 10.2312/EGWR/EGWR02/145-156
- [2] T. O. Aydin, R. Mantiuk, K. Myszkowski, and H.-P. Seidel. Dynamic range independent image quality assessment. *ACM Transactions on Graphics*, 27(3):69:1–69:10, 2008. doi: 10.1145/1360612.1360668
- [3] F. Drago, K. Myszkowski, T. Annen, and N. Chiba. Adaptive logarithmic mapping for displaying high contrast scenes. *Computer Graphics Forum*, 22(3):419–426, 2003. doi: 10.1111/1467-8659.00689
- [4] F. Durand and J. Dorsey. Fast bilateral filtering for the display of high-dynamic-range images. *ACM Transactions on Graphics*, 21(3):257–266, 2002. doi: 10.1145/566654.566574
- [5] R. Fattal, D. Lischinski, and M. Werman. Gradient domain high dynamic range compression. *ACM Transactions on Graphics*, 21(3):249–256, 2002. doi: 10.1145/566654.566573
- [6] S. Ferradans, M. Bertalmio, E. Provenzi, and V. Caselles. An analysis of visual adaptation and contrast perception for tone mapping. *IEEE Transactions on Pattern Analysis and Machine Intelligence*, 33(10):2002–2012, 2011. doi: 10.1109/TPAMI.2011.46
- [7] Z. Mai, H. Mansour, R. Mantiuk, P. Nasipoulous, R. Ward, and W. Heidrich. Optimizing a tone curve for backward-compatible high dynamic range image and video compression. *IEEE Transactions on Image Processing*, 20(6):1558–1571, 2011. doi: 10.1109/TIP.2010.2095866
- [8] R. Mantiuk, S. Daly, and L. Kerofsky. Display adaptive tone mapping. *ACM Transactions on Graphics*, 27(3):68:1–68:10, 2008. doi: 10.1145/1360612.1360667
- [9] R. Mantiuk and G. Krawczyk. pfstools: high dynamic range images and video. <http://pfstools.sourceforge.net/index.html>, 2019.

- [10] R. Mantiuk, K. Myszkowski, and H.-P. Seidel. A perceptual framework for contrast processing of high dynamic range images. *ACM Transactions on Applied Perception*, 3(3):286–308, 2006. doi: 10.1145/1166087.1166095
- [11] S. N. Pattanaik, J. Tumblin, H. Yee, and D. P. Greenberg. Time-dependent visual adaptation for fast realistic image display. In *Proceedings of the 27th Annual Conference on Computer Graphics and Interactive Techniques*, SIGGRAPH '00, pp. 47–54, 2000. doi: 10.1145/344779.344810
- [12] E. Reinhard and K. Devlin. Dynamic range reduction inspired by photoreceptor physiology. *IEEE Transactions on Visualization and Computer Graphics*, 11(1):13–24, 2005. doi: 10.1109/TVCG.2005.9
- [13] E. Reinhard, M. Stark, P. Shirley, and J. Ferwerda. Photographic tone reproduction for digital images. *ACM Transactions on Graphics*, 21(3):267–276, 2002. doi: 10.1145/566654.566575

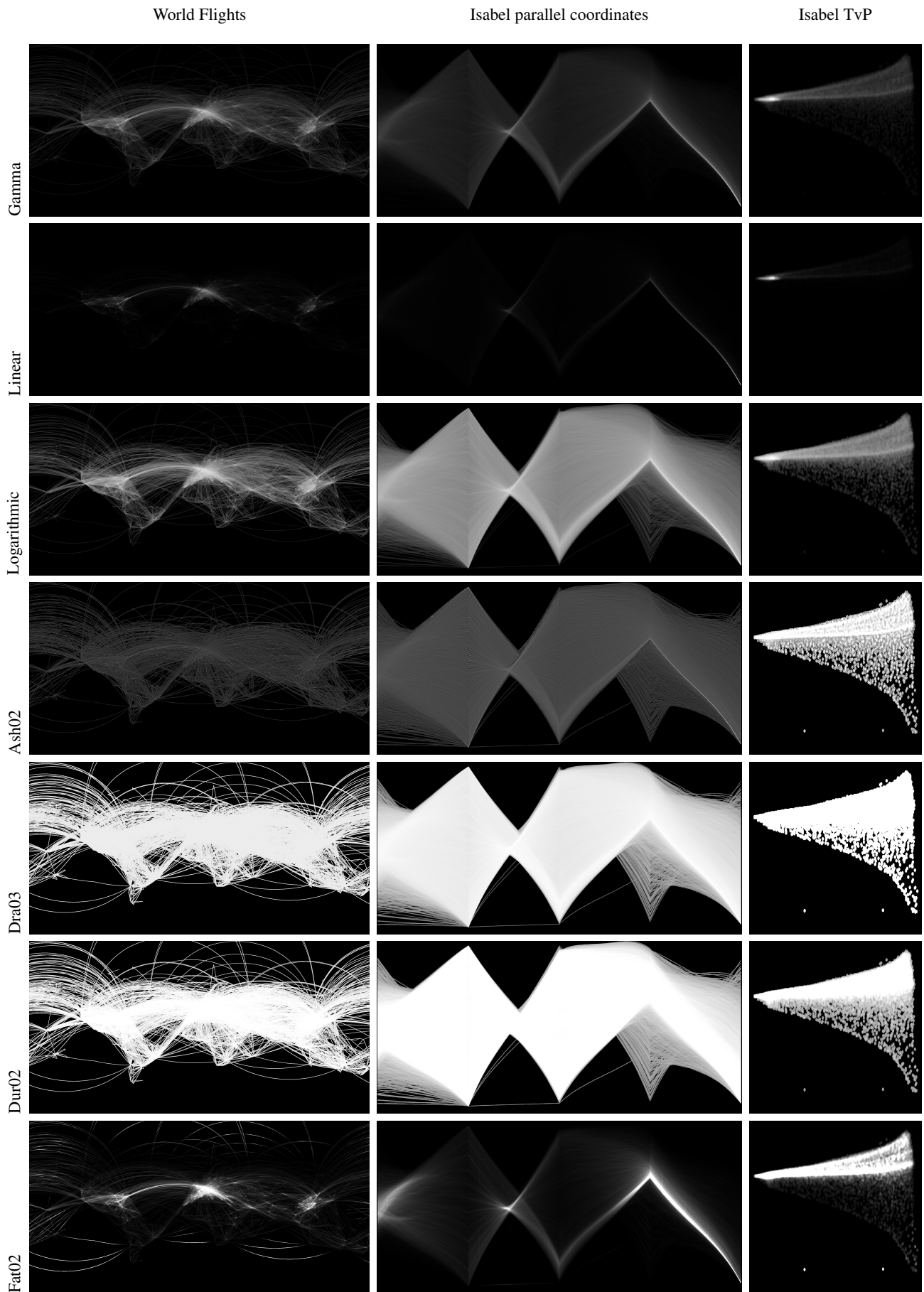


Figure 1: Tone-mapped images used in our evaluation: World flights (first row), Isabel parallel coordinates (second row), and the scatterplot of Hurricane Isabel TvP data (third row)

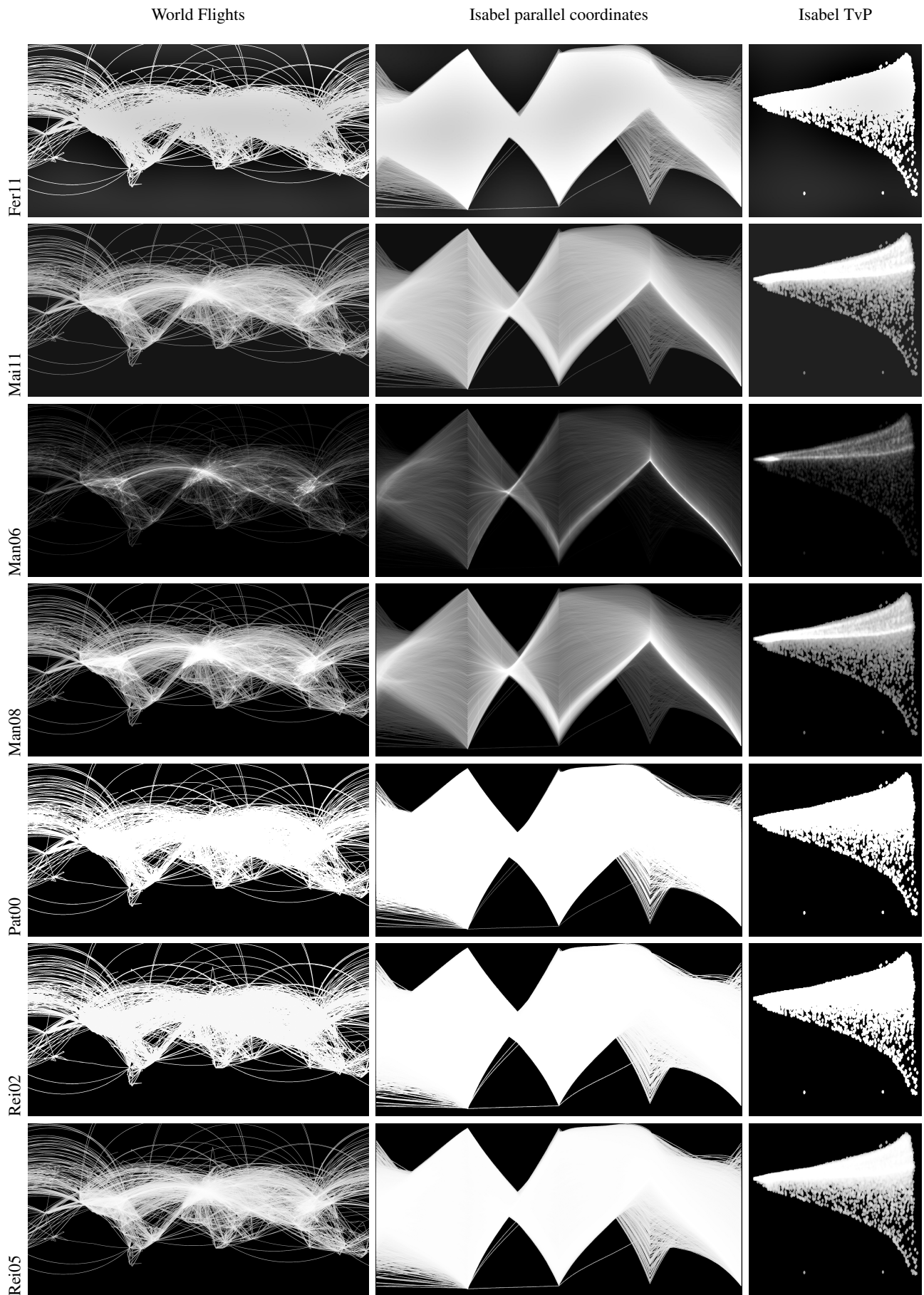


Figure 1: Continued figure from previous page.

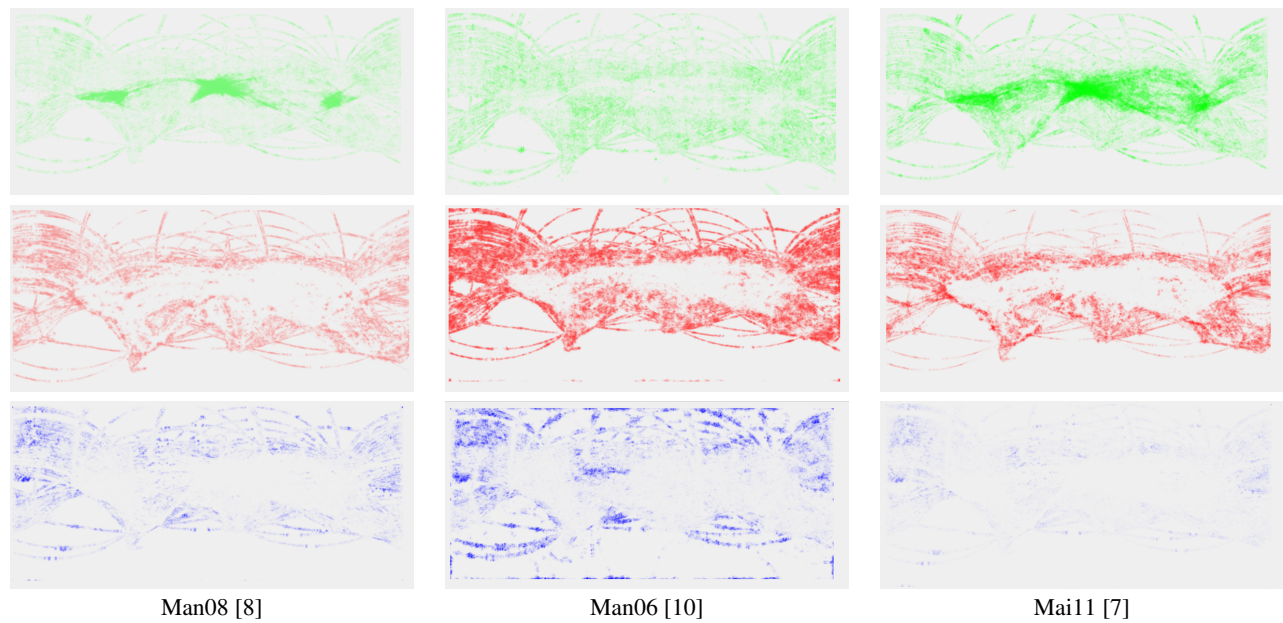


Figure 2: Distortion maps of the top three tone-mapping operators in our evaluation.